Unstable Waves on Oceanic Fronts: Large Amplitude Behavior and Mean Flow Generation

RICHARD A. WOOD

Department of Mathematics, University of Exeter, Exeter, U.K.

(Manuscript received 22 December 1986, in final form 2 December 1987)

ABSTRACT

A primitive equation numerical model is used to study the large amplitude behavior of unstable waves on an oceanic density front, concentrating on a single wave mode corresponding to the fastest growing linear solution. At small amplitude the model results agree well with linear theory, and at large amplitude "backward breaking" occurs and vortex pairs are formed, as have been observed in laboratory experiments. Vortex stretching due to advection across layer depth contours favors formation of the vortex pairs, with the result that the β effect is not necessary for vortex detachment, as it was in a previous, quasigeostrophic study by Ikeda.

Examination of the energetics allows a life cycle to be identified for the waves, and shows that kinetic energy is fed into the mean flow through Reynolds stress. It is shown that the β effect is important in determining the precise form of the mean flow generated, and this is interpreted in terms of the deep potential vorticity fluxes. For realistic parameters the mean flows generated agree well with observations of deep mean flows near the Gulf Stream; in particular there is a counterflow (westward) directly below the original position of the front and a positive (eastward) flow displaced to the south. This pattern is not found in the results of eddy-resolving general circulation models and is qualitatively different from the three-jet structure found in Ikeda's study of a symmetric, quasi-geostrophic jet.

1. Introduction

Surface density fronts are a common feature in the oceans, both over the continental shelf (Simpson 1981) and in the deep ocean, where the Gulf Stream is perhaps the best known example (Stommel 1966). Such fronts often exhibit transient wavelike or "meandering" motions, which can grow to large amplitude and eventually "pinch off" to form rings or eddies. These processes have been observed in the laboratory (Griffiths and Linden 1981, 1982) and in the ocean (Fuglister and Worthington 1951); they are of interest not only in their own right but also because both oceanic observations (Schmitz 1977) and the results of eddy-resolving general circulation models (Holland 1978; Holland and Rhines 1980) suggest that near the Gulf Stream the transient eddy field plays an important role in driving the mean flow.

Previous attempts to model the meandering process in mid-ocean fronts have been based on linear stability analysis (Killworth 1983; Garvine 1984; Killworth et al. 1984). While such studies are useful in providing a qualitative understanding of the dynamics of the meanders at small amplitude, their results cannot tell us a great deal about the large-amplitude behavior. Indeed Simmons and Hoskins (1978) found in modeling disturbances in the atmospheric jet stream that qualitatively different dynamics comes into play at large amplitudes, and that this can have an important effect on the interaction of the transient disturbances with the mean flow. This study uses a numerical model to study the properties of frontal waves at large amplitude.

Orlanski and Cox (1973) used a primitive equation numerical model in a periodic channel to study meanders in the Florida current. However, limitations on the computer power available at the time of their study meant that they were only able to carry out a small number of integrations, comparatively short in length and with a zonal resolution of about 20 km, scarcely fine enough to resolve the Rossby radius. This study uses a similar model to Orlanski and Cox, but we shall place particular emphasis on the type of large-amplitude meander found in the Gulf Stream between Cape Hatteras and Newfoundland (Hansen 1970; Apel 1980; Halliwell and Mooers 1983), although the model and the method could be applied to other frontal situations. In this region of the Gulf Stream the topography is much weaker than under the Florida Current, and the effects of topography are omitted from our model. The finite difference resolution in all directions is sufficient to resolve the Rossby radius, and the integrations are carried to a later stage of meander development than in Orlanski and Cox's study. Further, our methodology is slightly different in that we concentrate on the development of a single wavenumber mode instead of a

Corresponding author address: Dr. Richard A. Wood, Dept. of Mathematics, University of Southampton, Southampton SO9 5NH United Kingdom.

random perturbation with energy in all wavenumbers.

James (1984) used a similar modeling approach for meanders on shelf-sea fronts. Here mixing by wind and by tidal currents is more important than for deep ocean fronts, and accordingly James's results are directed toward studying the effect of various vertical mixing parameterizations on the development of the meanders. In the present study we concentrate on the detachment of eddies, on the energetics of the disturbances and on their interaction with the mean flow.

Attempts have been made to model the meanders, and in particular the eddy detachment process, using the quasi-geostrophic equations. Ikeda (1981) and Ikeda and Apel (1981) used a quasi-geostrophic numerical model to study the evolution of small perturbations to a symmetric, baroclinic jet, and recently Pratt and Stern (1986) have used contour dynamics to examine the process of eddy detachment from an isolated meander which is initially large, superposed on a stable basic state. Such studies provide important insights, but the quasi-geostrophic approximation precludes surface fronts and the primitive equations are necessary for a full dynamical description of frontal meanders. We shall see in section 4 that there are some discrepancies between our results and Ikeda's.

In section 2 of this paper we describe the numerical model and the experimental procedure. Section 3 compares wave properties at small amplitude with the linear theory of Killworth et al. (1984), and section 4 discusses finite amplitude effects. Section 5 identifies the stages in the life cycle of a disturbance in terms of the globally integrated energetics and section 6 discusses the mean flows generated by the disturbance and compares them with observations under the Gulf Stream. In section 7 we report on some studies of the parameter sensitivity and stability of our solutions, and finally section 8 is a summary and discussion of the results.

2. Method

Figure 1 shows schematically the domain of the model and its initial state. A two layer fluid is contained

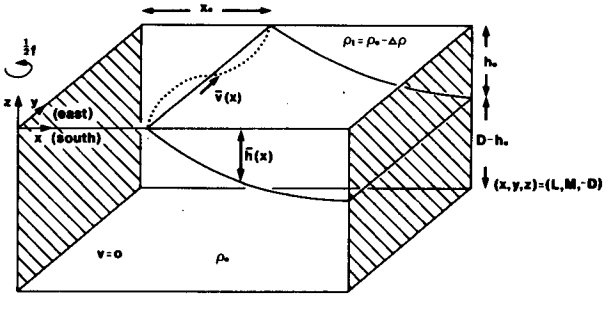

FIG. 1. The initial state of the model. Fluid of density $\rho_1 = \rho_0 - \Delta\rho$ overlies fluid of density ρ_0. The lower fluid is initially at rest, while in the upper fluid there is a velocity $\bar{v}(x)$ in geostrophic balance with the density field. The position X_0 of the surface outcrop varies sinusoidally with y in the initial state (dotted line).

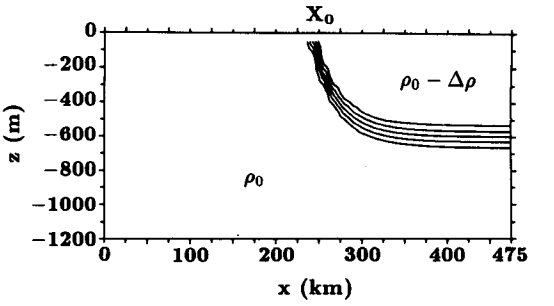

FIG. 2. Density contours for a cross-section across the channel (y = constant) in the initial state, for the shallow experiments. Contour interval $\Delta\rho/6$. The density difference $\Delta\rho$ is spread over a narrow thermocline region.

in a rotating channel of constant depth D, with rigid walls at $x = 0, L$ and a periodic boundary condition at $y = 0, M$. There is no thermodynamic or wind forcing. The interface profile $\bar{h}(x)$ intersects the surface at $x = X_0$ in a front; the particular profile chosen for all the experiments presented here is

$$\bar{h}(x) = \begin{cases} 0, & x < X_0 \\ h_0(1 - \exp((X_0 - x)/a)), & x \geq X_0 \end{cases}$$

where $a = [g\Delta\rho h_0/(\rho_0 f^2)]^{1/2}$ is the Rossby radius and g, $\Delta\rho$, ρ_0 and f take their usual meanings. Provided the front is far from the wall $x = L$ (compared with a), $\bar{h}$ is approximately h_0 at the wall. Assuming f is constant, this choice of $\bar{h}$ results in uniform potential vorticity $(f + \bar{v}_x)/\bar{h}$ in the upper layer if a basic flow $\bar{v}(x)$ is prescribed in geostrophic balance with $\bar{h}$, as in the Gulf Stream model of Stommel (1966, p. 109).

To initiate unstable waves, a small, sinusoidal variation is imposed on the frontal position X_0 in the initial state (Fig. 1); thus at $t = 0$:

$$X_0(y) = \bar{X}_0 + \epsilon \sin(2\pi y/M)$$

where $\bar{X}_0$ is the mean value and ϵ is chosen to be equal to the horizontal grid interval Δx.

We integrate the primitive equations:

$$u_t + \mathbf{u}\cdot\nabla u - fv = -p_x/\rho_0 + A_H(u_{xx} + u_{yy}) + A_V u_{zz} \quad (2.1)$$

$$v_t + \mathbf{u}\cdot\nabla v + fu = -p_y/\rho_0 + A_H(v_{xx} + v_{yy}) + A_V v_{zz} \quad (2.2)$$

$$p_z = -\rho g \quad (2.3)$$

$$\nabla\cdot\mathbf{u} = 0 \quad (2.4)$$

$$\rho_t + \mathbf{u}\cdot\nabla\rho = K_H(\rho_{xx} + \rho_{yy}) + K_V\rho_{zz} \quad (2.5)$$

where $\mathbf{u} \equiv (u, v, w)$ is the velocity, p the pressure and ρ the density. Figure 2 shows a cross section through the initial density field at constant y; initial velocities are calculated by integrating the thermal wind equation

TABLE 1.

Designation	Description	D (m)	f_0 (s^{-1})	β ($m^{-1}\,s^{-1}$)	M (km)	Length of integration (days)
SF	Shallow f-plane	1200	10^{-4}	0	180	28
SB	Shallow β-plane	1200	10^{-4}	1.50×10^{-10}	180	28
DF	Deep f-plane	4000	10^{-4}	0	270	60
DB	Deep β-plane	4000	10^{-4}	1.57×10^{-11}	270	79

vertically up from the bottom (where the velocity is taken to be zero initially). Notice that instead of the interface in Fig. 1 we have a thin "thermocline" region (resolved by at least two finite difference grid intervals). In much of what follows it is convenient to interpret the results in terms of a two-layer system—where this happens we shall identify the depth of the $\rho = \rho_0 - \Delta\rho/2$ isopycnal surface in the model (found by linear interpolation on the ρ values stored on the model grid) with the interface depth h in the two-layer system. Exhaustive testing in cases where the two-layer system can be solved analytically (Wood 1988) suggests that the evolution of the given isopycnal surface in the numerical model does follow closely the evolution of the interface in the two-layer system, notwithstanding some discrepancies found by Cooper (1986) when the thermocline region was more poorly resolved than here. By adopting this approach we avoid problems in following the frontal outcrop, which would arise (for example when cutoff eddies were formed) if we were to integrate the two-layer shallow water equations, allowing the interface to intersect the surface.

The numerical method used follows that of Bryan (1969), but terms in Bryan's formulation involving topography, which are identically zero in our flat bottomed domain, are omitted, thus reducing the computational cost. "Free slip" boundary conditions are applied at the walls ($u = v_x = 0$) and at the bottom ($u_z = v_z = w = 0$), and "adiabatic" boundary conditions are applied to ρ ($\rho_x = 0$ at the walls, $\rho_z = 0$ at the surface and the bottom). For all the experiments presented here h_0 is taken as 600 m, and the density anomaly $\Delta\rho$ is chosen to give the Rossby radius $a = 30$ km. Horizontal grid spacing is chosen to resolve a, with typical values $\Delta x = 7$ km, $\Delta y = 9$ km; vertical grid spacing Δz is 100 m in the uppermost 800 m, with coarser resolution at deeper levels (where the density stratification does not penetrate). For the experiments described in this paper vertical and horizontal eddy viscosities and diffusivities $A_V = K_V = 10^{-3}\ m^2\ s^{-1}$ and $A_H = K_H = 200\ m^2\ s^{-1}$ are used. In section 7 we discuss the sensitivity of the results to the choice of these constants. A typical value for the channel width L is 735 km = $(24.5)a$; experiments with various values of L confirm that the results presented here are not affected by the presence of the walls. The Coriolis parameter f is allowed to vary with x as $f = f_0 - \beta x$, so that in our coordinate system the negative x-direction represents north; the results of section 6 show that the β effect is important in controlling the mean flows induced by the frontal disturbances.

Table 1 gives parameters for the four main experiments presented here. In both "deep" and "shallow" cases the channel length M (and hence the wavelength) is chosen to be close to the wavelength of the fastest growing wave according to the linear f-plane theory of Killworth et al. (1984). Parameter values for the deep runs are chosen to resemble the Gulf Stream northeast of Cape Hatteras, and to allow comparison with the published results of Killworth et al. (1984). For run SB a large value of β is chosen so as to produce significant variation of the lower layer potential vorticity $f/(D - \bar{h})$ on the scale of the Rossby radius; we shall see the importance of this in section 6.

3. Comparison with linear theory

In this section we compare the small amplitude behavior of the unstable waves observed in our numerical model with the linear f-plane theory of Killworth et al. (1984, hereafter referred to as KPS). This study appears to be the most appropriate to date for Gulf Stream meanders since it is the only one which includes an active lower layer; with Gulf Stream parameters this can make a considerable difference to the growth rates obtained.

a. Growth rate

Growth rates were calculated using centered difference approximations to $d/dt(\log A)$, where A is the amplitude (i.e. half the maximum x-variation) of the $h = 150$ m contour, and h is the notional interface depth as defined in section 2. For the shallow f-plane case, several values of M (wavelengths) were tried, ranging from 108 km ($\epsilon \approx 1.75$ in the notation of KPS) to 270 km ($\epsilon \approx 0.7$); the growth rates agreed well with values obtained from Fig. 4 of KPS, with the short-wave cutoff being reproduced and all nonzero growth rates lying within 11% of the KPS results (see Fig. 3). The deep case is more expensive computationally because of the slower growth and longer wavelength, so only the case $M = 270$ km (the fastest growing wave according to KPS) was run (experiment DF); the growth rate measured was 0.23 $days^{-1}$ compared with 0.26 $days^{-1}$ derived from the results of KPS.

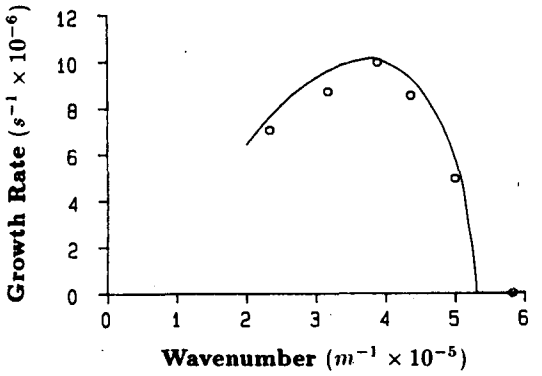

FIG. 3. Growth rates as a function of wavenumber, for experiment SF. The solid curve is derived from the linear calculations of Killworth et al. (1984), the open circles are values measured from the present model.

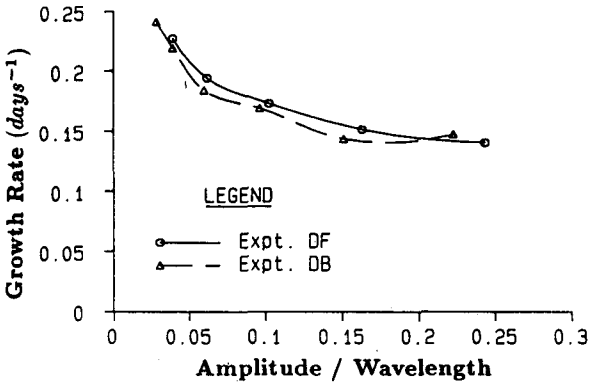

FIG. 4. Growth rate shown as a function of amplitude for experiments DF and DB.

Inclusion of the β effect had a stabilizing influence in both deep and shallow cases, as in Orlanski and Cox (1973). For the deep run the growth rate was reduced by about 4% (to 0.22 days^{-1}).

b. Phase speed

Phase speeds were calculated in two ways, based on the positions of the trough (maximum x value) and of the crest (minimum x value) of the $h = 150$ m contour. For experiment SF (with wavelength $M = 180$ km) the initial phase speed was 30.3 cm s^{-1} for the trough and 30.8 cm s^{-1} for the crest, compared with a value of about 30.5 cm s^{-1} derived from KPS. For experiment DF the phase speed was 13.2 cm s^{-1} for both trough and crest, while KPS quote about 13 cm s^{-1}.

Inclusion of the β effect reduced the phase speed in both experiments, by about 5% (to 12.8 cm s^{-1} (trough), 12.4 cm s^{-1} (crest)) in the deep case.

We conclude that the dominant unstable mode observed in the model runs is well described by the linear theory of KPS at small amplitude; for the shallow case we have demonstrated this agreement over a wide range of wavelengths M. We now restrict our attention to the fastest growing wave for our study of finite amplitude effects.

4. Finite amplitude behavior

Observations of Gulf Stream meanders (Apel 1980; as interpreted by Ikeda 1981 and by Ikeda and Apel 1981) suggest that both the growth rate and the phase speed tend to decrease as the amplitude of the meander increases. Figures 4 and 5 show growth rate and phase speed of the growing wave (calculated as described in section 3) as functions of its amplitude, for the deep experiments DF and DB, and we see that both quantities decrease as the amplitude increases. The phase speed based on the position of the crest behaves differently from the phase speed based on the position of the trough: the trough speed levels off at between half and two thirds its small amplitude value, whereas the crest speed decays more rapidly and continues to decay, with the result that the trough catches up with the crest.

At large amplitude, James (1984) reported a sharpening of the front in certain regions. In our results such a sharpening occurs near the wave trough, accompanied by a weakening of the front (i.e., a reduction in the size of ∇h) at the crest. At very large amplitude (Fig. 6) the wave adopts the backward breaking shape familiar from laboratory experiments (e.g., Griffiths and Linden 1982), and eventually pinches off a cyclonic/anticyclonic vortex pair. The closed cyclonic (cold) circulation forms first and initially has a velocity signature extending to the bottom, while the anticyclonic (warm) circulation forms later and is surface intensified; these results agree with Griffiths and Linden's (1981) laboratory observations. However the deep flow signature of the cyclonic vortex soon disappears as it interacts with the mean flow, producing the deep flows discussed in section 6.

As the meander grows, we observe large vertical velocities (of order 10^{-3} m s^{-1} in experiment DB) near

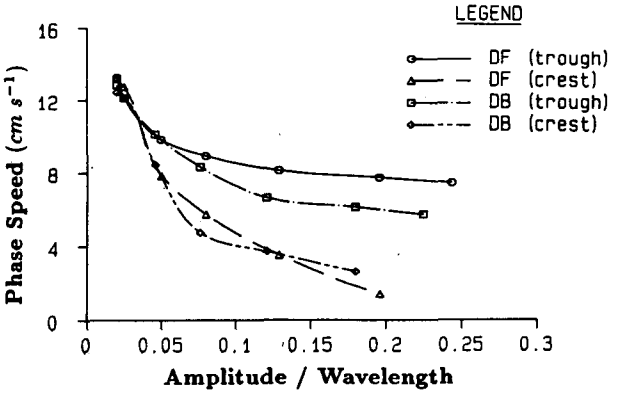

FIG. 5. Phase speed of the wave crest and of the wave trough, shown as a function of amplitude for experiments DF and DB.

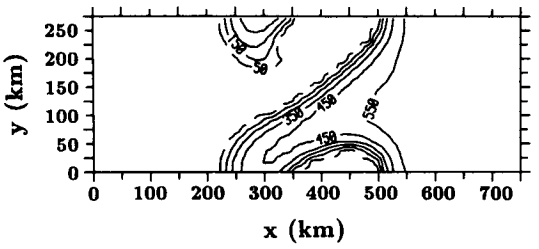

FIG. 6. Contours of interface depth h vs (x, y) for experiment DB after 25 days of integration. Contours are at 50 m (dashed), then at intervals of 100 m down to 550 m.

the front. The phase of the vertical velocity lags that of the frontal displacement by approximately $\pi/2$, with upwelling behind the crest and downwelling ahead of it. These results agree well with recent observations of a Gulf Stream meander by Levine et al. (1986). The largest vertical velocities (up to 1.6×10^{-3} m s^{-1}) appear to occur around the time when the cyclonic vortex is pinched off (Fig. 6). There is also evidence of a small-scale cross-frontal circulation cell, with upwelling at the front and downwelling just ahead of it; a similar circulation can be seen in some of the results of James (1984).

Comparing our results with Ikeda's (1981) study of meanders in a symmetric, quasigeostrophic jet, we see that:

(i) Ikeda found a linear dependence of both growth rate and phase speed on the square of the amplitude, for amplitudes less than about 0.2 of a wavelength. Our results show no such dependence; indeed we were unable to fit any power law relationship to the data.

(ii) Ikeda (1981) and Orlanski and Cox (1973) found that the growth rate in the f-plane case eventually decayed to below that in the β-plane case. Our results show the same behavior.

(iii) In Ikeda's study the phase speed (based on the extremes of the meander) decreased almost to zero by the time the amplitude reached 0.3 of a wavelength. As can be seen from Fig. 5, in our case this is true for the crest but not for the trough. Further, the crest phase speed in the f-plane case decays to below that in the β-plane case, as suggested by Ikeda's results, but this does not happen for the trough. In these respects our trough phase speed behaves in a similar way to the phase speed of the zero crossings in Ikeda's model.

(iv) In Ikeda's study the β effect was necessary for cutoff eddies to form. This is not the case in our results, as shown in Fig. 7a. Indeed the β effect appears to trap the cyclonic (cold) eddy near the front, as shown in Fig. 7b. We shall return to this trapping effect when we consider the evolution of the mean flow in section 6.

To explain the discrepancies (iii) and (iv) between our results and Ikeda's, we must consider the main differences between the two models, viz. the different basic states (asymmetric, exponential jet vs symmetric, gaussian jet) and the different dynamical equations (primitive equations, with large interface displacements, vs quasi-geostrophic). Note that in Ikeda's model the combination of symmetric basic state and quasigeostrophic dynamics constrains the wave crest and trough to behave identically.

It is plausible to explain the evolution of the phase speed, as described in (iii) above, in terms of differential advection by the sheared basic flow. In Ikeda's case the crest and trough rapidly move into regions of very small basic flow as the wave grows, and so are not advected downstream as fast as the zero crossings, which stay in the region of maximum basic flow. This accounts for the symmetric backward breaking seen in Ikeda's results. In our case the crest is in a region of zero basic flow, and so is not advected, whereas the trough remains for some time in a region where the basic flow is reasonably strong (the basic flow decays more slowly away from the jet maximum than it does in Ikeda's case) and so the trough *is* advected. The zero crossings are in the region of strongest basic flow, and their phase speed (not shown) levels off at a somewhat larger value than the trough phase speed.

To explain the fact that β is not necessary for eddy detachment in our case, whereas it was in Ikeda's [see (iv) above] we have carried out a detailed diagnostic study (see Wood 1988 for the details). In Ikeda's model the principal mechanism by which the relative vorticity of a fluid parcel is changed is conservation of potential vorticity as the parcel is advected up or down the planetary vorticity gradient (i.e., the β term); this leads to the production of anticyclonic relative vorticity at the crest and cyclonic relative vorticity at the trough. Vor-

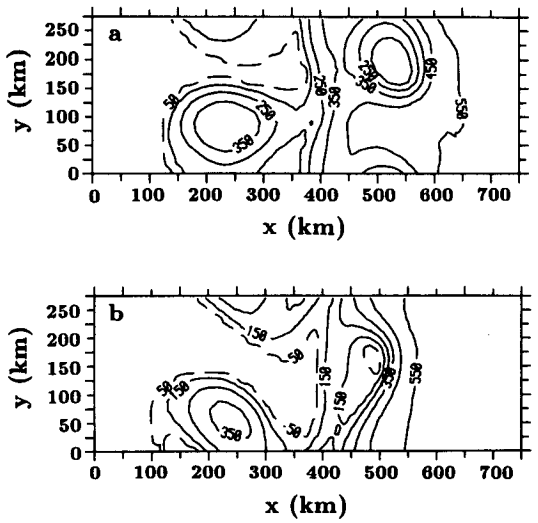

FIG. 7. Contours of interface depth h vs (x, y) for (a) experiment DF after 46 days, and (b) experiment DB after 50 days. Contour levels as for Fig. 6.

tex stretching as fluid parcels are advected into regions of differing layer thickness is negligible. In contrast, for our case it is the vortex stretching terms which dominate. This is because variations in layer thicknesses are much larger, and because vortex stretching due to the *ageostrophic* component of the flow is allowed by the primitive equations (this ageostrophic term does not appear in the quasi-geostrophic equations, but in some regions of our model domain it is as large as the vortex stretching due to geostrophic advection). The vortex stretching again induces anticyclonic relative vorticity at the crest and cyclonic relative vorticity at the trough, and is sufficient to induce eddy formation without the help of β.

5. Energetics and life cycle

To understand the development of the disturbance it is useful to look at the energetics of the system. All prognostic variables are split into a zonal (y) mean component (denoted by an overbar) and a departure from that mean (denoted by a prime and referred to as the perturbation or eddy component). From (2.1)–(2.5) we can form evolution equations for the total kinetic energy of the mean flow, the total kinetic energy of the perturbation flow, and the total gravitational potential energy, in the usual way (as, for example, in Orlanski and Cox 1973), giving in our case:

$$\frac{d}{dt}\int \tfrac{1}{2}(\bar{u}^2+\bar{v}^2)dV$$

$$= -\int (\bar{u}\overline{u'u'_x} + \bar{u}\overline{w'u'_z} + \bar{v}\overline{u'v'_x} + \bar{v}\overline{w'v'_z})dxdz$$

$$- \int \frac{g}{\rho_0}\bar{w}\bar{\rho}dxdz - \int A_H(\bar{u}\bar{u}_{xx} + \bar{v}\bar{v}_{xx})$$

$$+ A_V(\bar{u}\bar{u}_{zz} + \bar{v}\bar{v}_{zz})dxdz \quad (5.1)$$

$$\frac{d}{dt}\int \tfrac{1}{2}(\overline{u'^2} + \overline{v'^2})dV$$

$$= +\int (\bar{u}\overline{u'u'_x} + \bar{u}\overline{w'u'_z} + \bar{v}\overline{u'v'_x} + \bar{v}\overline{w'v'_z})dxdz$$

$$- \int \frac{g}{\rho_0}\overline{w'\rho'}dxdz$$

$$- \int A_H(\overline{u'u'_{xx}} + \overline{u'u'_{yy}} + \overline{v'v'_{xx}} + \overline{v'v'_{yy}})$$

$$+ A_V(\overline{u'u'_{zz}} + \overline{v'v'_{zz}})dxdz \quad (5.2)$$

$$\frac{d}{dt}\int \frac{g}{\rho_0}\rho z dV = \int \frac{g}{\rho_0}\bar{w}\bar{\rho}dxdz + \int \frac{g}{\rho_0}\overline{w'\rho'}dxdz$$

$$+ \int -K_V\frac{g}{\rho_0}\rho_z dV \quad (5.3)$$

We write these symbolically as

$$\frac{d}{dt}(\overline{\mathrm{KE}})$$

$$= -(\overline{\mathrm{KE}} \rightarrow \mathrm{KE}') + (\mathrm{PE} \rightarrow \overline{\mathrm{KE}}) + (A \rightarrow \overline{\mathrm{KE}}) \quad (5.4)$$

$$\frac{d}{dt}(\mathrm{KE}')$$

$$= (\overline{\mathrm{KE}} \rightarrow \mathrm{KE}') + (\mathrm{PE} \rightarrow \mathrm{KE}') + (A \rightarrow \mathrm{KE}') \quad (5.5)$$

$$\frac{d}{dt}(\mathrm{PE})$$

$$= -(\mathrm{PE} \rightarrow \overline{\mathrm{KE}}) - (\mathrm{PE} \rightarrow \mathrm{KE}') + (\mathrm{KV} \rightarrow \mathrm{PE}). \quad (5.6)$$

Where $(\overline{\mathrm{KE}} \rightarrow \mathrm{KE}')$ represents the transfer of kinetic energy between the mean and eddy fields via Reynolds stresses, $(\mathrm{PE} \rightarrow \overline{\mathrm{KE}})$ and $(\mathrm{PE} \rightarrow \mathrm{KE}')$ the conversion of gravitational potential energy to kinetic energy of the mean and eddy fields, $(A \rightarrow \overline{\mathrm{KE}})$ and $(A \rightarrow \mathrm{KE}')$ the viscous dissipation of kinetic energy (these terms are always negative in the absence of wind or other surface stress forcing) and $(\mathrm{KV} \rightarrow \mathrm{PE})$ the gain of potential energy due to vertical eddy diffusion (always positive for a stably stratified fluid, but generally small in our experiments).

Figure 8a shows $\overline{\mathrm{KE}}$, KE′ and PE as functions of time, for experiment SB. Figure 8b shows the transfer terms on the right hand side of (5.4)–(5.6), on the same time scale. The behavior in the first half of the experiment (up to 13 days) is common to all the experiments and consists of a baroclinic growth phase during which KE′ increases at the expense of PE, followed by a second phase in which strong Reynolds stress convergences feed a mean flow $[(\overline{\mathrm{KE}} \rightarrow \mathrm{KE}') < 0]$. During this second phase, which coincides with the pinching off of the vortex pair, potential energy extraction declines. This cycle in the energetics is similar to those found by Ikeda (1981), and in the context of the atmospheric jet stream by Simmons and Hoskins (1978).

The behavior after these first two phases is rather more variable between the experiments, but we always observe a damped oscillatory behavior in $(\overline{\mathrm{KE}} \rightarrow \mathrm{KE}')$ and in $(\mathrm{PE} \rightarrow \mathrm{KE}')$, with $(\mathrm{PE} \rightarrow \mathrm{KE}') \approx -(\overline{\mathrm{KE}} \rightarrow \mathrm{KE}')$ so that the potential energy extracted feeds $\overline{\mathrm{KE}}$ (via the indirect route of the Reynolds stress term) rather than KE′. Superimposed on this is a weak barotropic instability $[(\overline{\mathrm{KE}} \rightarrow \mathrm{KE}') > 0]$ of the newly generated mean flow; this barotropic instability is somewhat enhanced when the system is free to oscillate at wavelengths longer than the initial wavelength of the disturbance (see section 7).

Two other notable features can be seen in the energetics:

(i) During the baroclinic growth phase there is considerable wave activity at the inertial frequency, which can be seen as the high frequency signal in $(\mathrm{PE} \rightarrow \mathrm{KE}')$ and $(\mathrm{PE} \rightarrow \overline{\mathrm{KE}})$ in Fig. 8b; this may be due to the near-

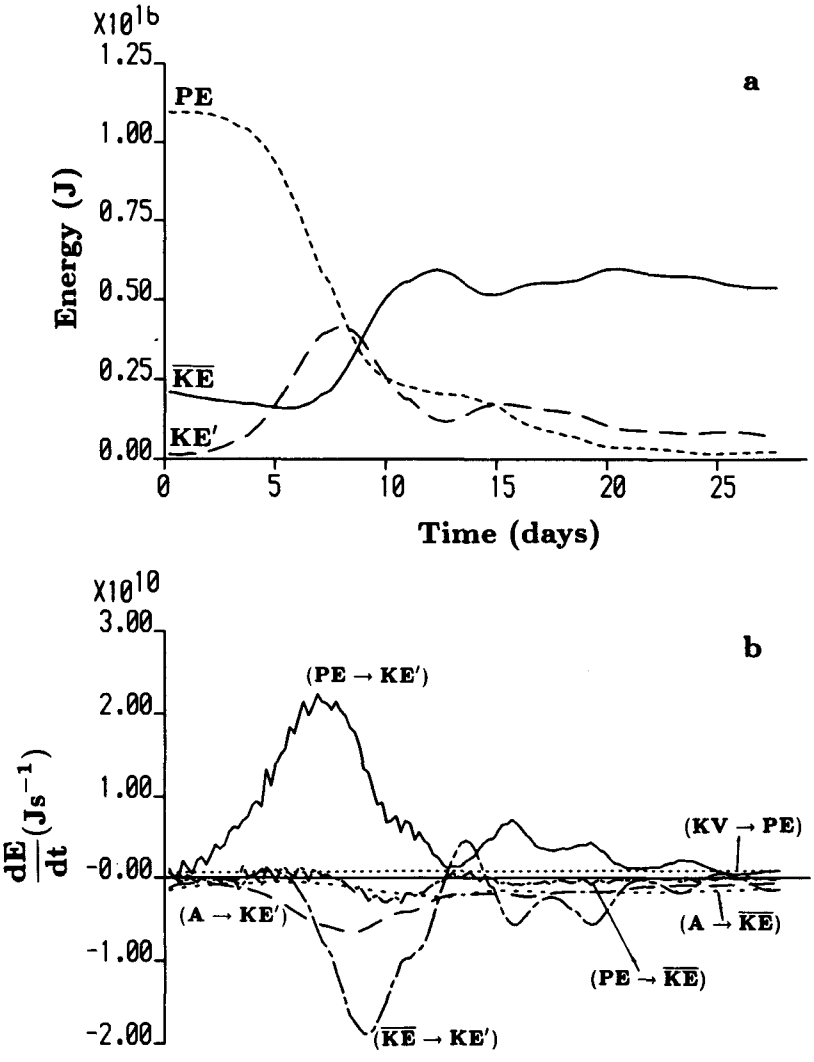

FIG. 8. (a) The potential energy PE, and the mean and fluctuation components of the kinetic energy, $\overline{KE}$ and KE', as functions of time for experiment SB. (b) Energy transformation terms for the same experiment (same time scale).

inertial frontally-trapped modes investigated by Paldor (1983). This inertial activity stops during the "Reynolds stress" phase, in most cases rather suddenly (as in Fig. 8b after about 11 days).

(ii) Figure 9 shows the proportion of the total kinetic energy due to the barotropic component of the flow, as a function of time, for experiment SB. We see a monotonic rise from an initial value of around 0.3, leveling off at a more or less steady value of about 0.87 by the end of the Reynolds stress phase. For experiment DB the proportion at the end of the integration (79 days) is about 0.89, but it is still rising slowly at this stage.

6. Induced mean flows

We saw in section 5 that around the time when the vortex pair pinches off there is an increase in the kinetic energy of the mean flow, due to Reynolds stresses. In this section we shall examine the process in more detail, concentrating on the deep flows.

Figure 10a shows deep velocity vectors for experiment DB after 25 days of integration (Fig. 6 shows the h field at the same time); the dominant feature is the strong cyclonic circulation associated with the cold eddy. By the end of the integration (79 days, Fig. 10b) the dominant pattern is of two oppositely directed meandering jets, a negative (westward flowing) jet directly below but centered somewhat to the north of the original position of the front and a slightly stronger, narrower, positive (eastward flowing) jet to the south. This double jet structure establishes itself as the vortex pair separates from the front, and can be identified easily by day 33 (which is towards the end of the Reynolds stress phase in the energetics).

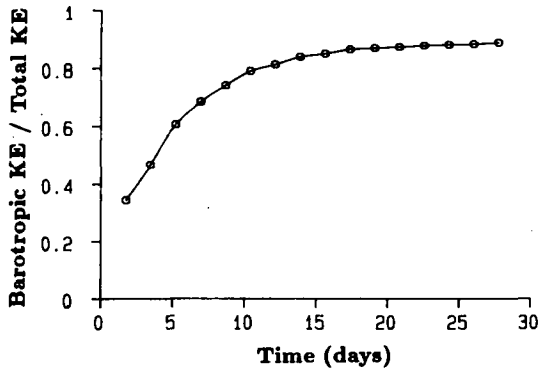

FIG. 9. The proportion of the total kinetic energy due to the barotropic mode, as a function of time, for experiment SB.

The evolution of the jets in time depends on the value of β. Figure 11 shows the deep, zonal (y) mean zonal velocity $\bar{v}$ as a function of x and t, for the shallow experiments SF and SB. In the f-plane case the eastward jet moves out to the right at approximately constant speed, and experiments not shown here suggest that it continues to do so until it reaches the wall $x = L$; the position of the westward jet, however, is roughly constant in time. In contrast to the β-plane case the eastward jet initially moves to the right (southwards) but then appears to reach an equilibrium position. The position of the westward jet is not greatly affected by β. Both the eastward and the westward jets are considerably weaker in the β-plane case than in the f-plane case. Figure 12 shows $\bar{v}$ against x and t for experiment DB. The maximum velocities in the jets are -0.25 and $+0.30$ m s^{-1} and the jet cores are situated about 80 km north and 150 km south of the original position of the front. However, the strengths (but not the positions) of the jets are sensitive to the choice of the eddy viscosity A_H (see section 7).

It is interesting to interpret the migration of the deep jets in terms of the lower layer potential vorticity $q_2 = (v_{2x} - u_{2y} + f)/(D - h)$, where u_2, v_2 are the velocity components in the lower layer. Figure 13a shows the mean profiles $\bar{q}_2$ against x (the north–south coordinate) in the initial state, for experiments DF and DB. The front separates fluid of lower potential vorticity to the left (north) from fluid of higher potential vorticity to the right (south). As the disturbance develops upper layer fluid is transported from south to north across the original position of the front, and in order to conserve volume some lower layer fluid must be transported from north to south; thus low potential vorticity fluid must be mixed across the front in the lower layer. This mixing of potential vorticity can be seen clearly in Fig. 13b, where after 25 days a negative anomaly in $\bar{q}_2$ has developed in the high $\bar{q}_2$ region to the south, and a positive anomaly has developed in the low $\bar{q}_2$ region to the north. The negative anomaly in $\bar{q}_2$ (which is associated with the cold eddy) propagates to the south. In the f-plane case it continues until it reaches the wall $x = L$, while in the β-plane case it comes to rest with its minimum near the position of the original maximum of $\bar{q}_2$ (there is no such maximum in the f-plane case). This is consistent with the cold eddy acting as a diffuser of $\bar{q}_2$, in the sense that placing the associated bowl-shaped negative anomaly under the maximum of the original profile minimizes $\int (\bar{q}_{2x})^2 dx$. In contrast the maximum associated with the anticyclonic vortex moves to the left past the initial minimum of $\bar{q}_2$, and eventually smaller-scale instabilities complicate the picture (67 days, Fig. 13b).

To examine in more detail the processes responsible for generating the mean flows we have examined the individual terms in the equation of motion for the zonal mean, zonal flow $\bar{v}$:

$$\bar{v}_t = -(\bar{u}\bar{v})_x - (\overline{u'v'})_x - (\bar{w}\bar{v})_z - (\overline{w'v'})_z - f\bar{u} + A_H\bar{v}_{xx} + A_V\bar{v}_{zz} \quad (6.1)$$

for experiment DB after 25 days of integration (during the Reynolds stress phase, when the deep flows are being established). The dominant terms are the horizontal Reynolds stress divergence $-(\overline{u'v'})_x$ and the Coriolis acceleration due to the mean cross-stream flow, $-f\bar{u}$. These are shown in Fig. 14a, b. Near the surface the two terms are almost equal and opposite; this near-balance of the Reynolds stress divergence and Coriolis terms was noted by Phillips (1956) in his study of the atmospheric general circulation. As depth increases $\bar{u}$ changes sign and at depth the two terms are of the same sign. The acceleration due to Reynolds stress is of order 1 cm s^{-1}/day, of the same order of magnitude

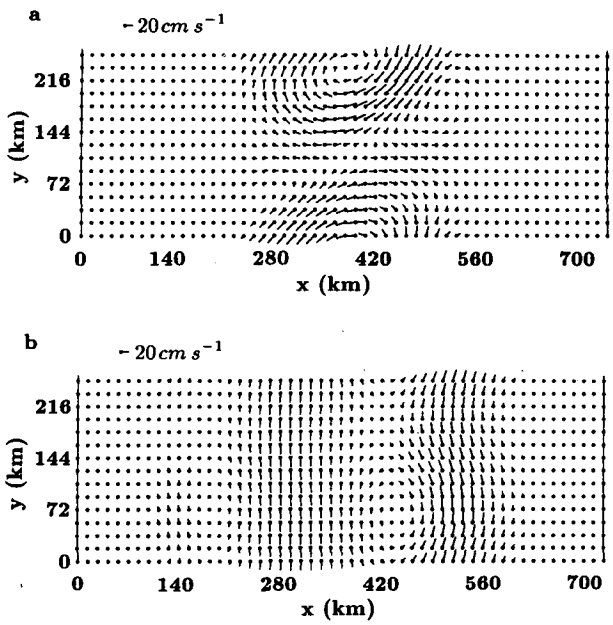

FIG. 10. Velocity vectors at 3250 m depth for experiment DB after (a) 25 days, and (b) 79 days. Vectors point away from the dots.

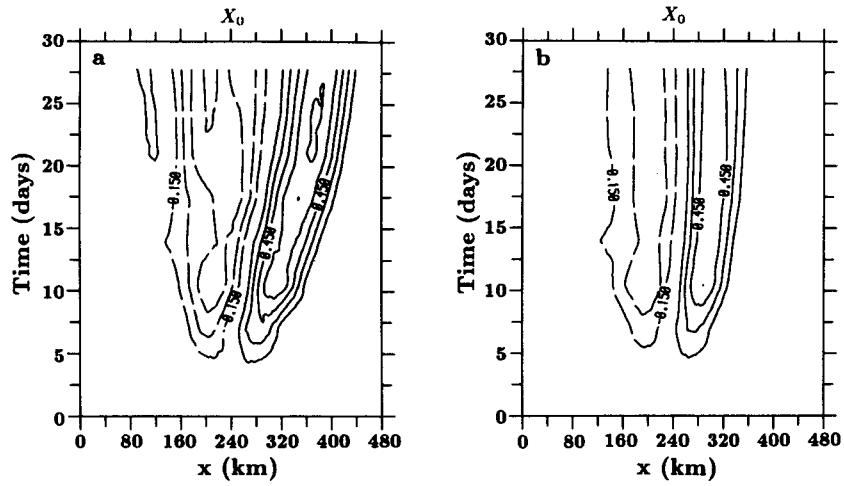

FIG. 11. Contours of the mean velocity $\bar{v}$ at 1150 m depth, against (x, t) for (a) experiment SF, and (b) experiment SB. Contour interval 0.15 m s^{-1}. Broken contours denote negative values.

as the value found by Luyten (1977) in observations over the continental rise, although there topographic Rossby waves are thought to have an important influence (Hogg 1981). Figure 14c shows the sum of $-(\overline{u'v'})_x$ and $-f\bar{u}$, and we can see that these two terms account for most of $\bar{v}_t$ (shown in Fig. 14d).

Our results for experiment DB (Fig. 12) show several similarities with Schmitz's (1977) observations of deep velocities under the Gulf Stream. In particular Schmitz observed a westward flowing jet directly below and to the north of the Gulf Stream axis, and a stronger and perhaps narrower eastward jet (the spatial resolution of the measurements is not adequate to be sure of its width) about 150 km south of the axis. There is no evidence in our results of the second westward jet seen further to the south in Schmitz's observations. We do however notice a weaker eastward jet (with maximum velocity about 0.07 m s^{-1}) developing from about day 55 to the north of the main westward jet; this is outside the domain of Schmitz's observations. The model velocities are about a factor of 3 larger than Schmitz's data at 55°W; however comparison of the maximum of our instantaneous spatial mean with Schmitz's long-time mean data is not straightforward, and the model values are in any case sensitive to the choice of A_H (section 7).

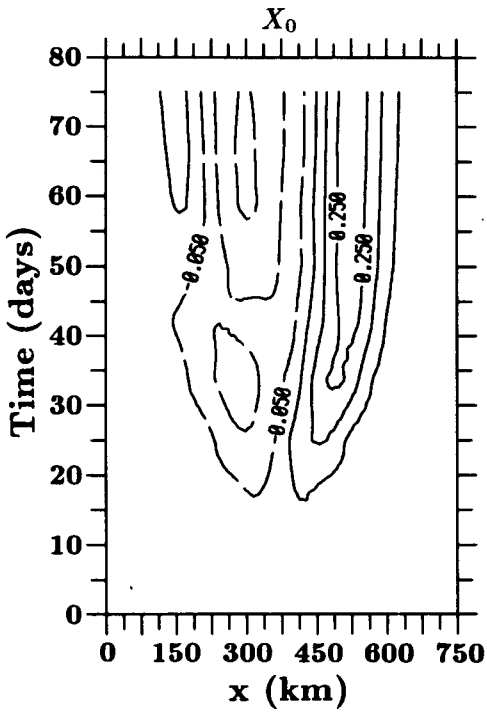

FIG. 12. Contours of the mean velocity $\bar{v}$ at 3250 m depth, against (x, t), for experiment DB. Contours at ±0.05 m s^{-1}, then at intervals of 0.1 m s^{-1}. Broken contours denote negative values.

7. Further experiments

a. Sensitivity to A_H and K_H

Recently Holland and Batteen (1986) have shown how, in the context of a quasi-geostrophic general circulation model, horizontal diffusion of heat (density) can play an important role in modifying the eddy field. To investigate the role of horizontal eddy diffusion and viscosity in our model, we have carried out a series of experiments with parameter values as for experiment SB, but with various values for K_H and A_H in the range 20–400 m^2 s^{-1}. The results may be summarized as follows (for further details see Wood 1988):

(i) The evolution of the flow fields as described in section 4 is not changed qualitatively for K_H, A_H in the given range.

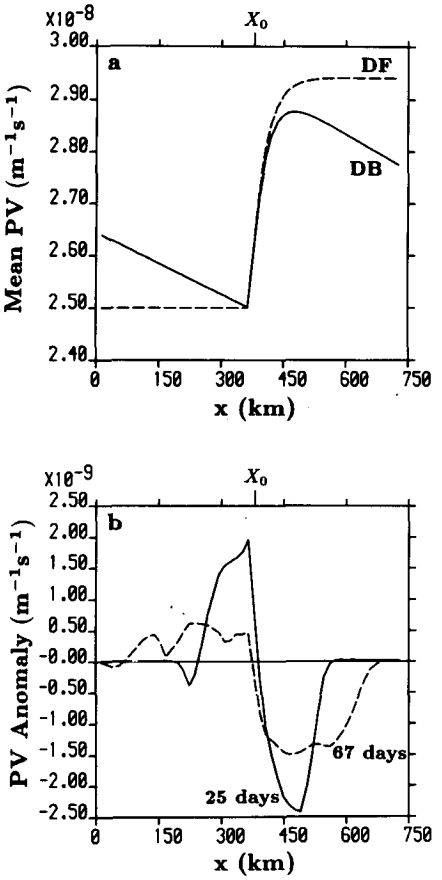

FIG. 13. (a) Mean lower layer potential vorticity $\bar{q}_2$ in the initial state, for experiments DF (dashed) and DB (solid). (b) Potential vorticity anomaly $\bar{q}_2 - \bar{q}_2|_{t=0}$ for experiment DB after 25 days (solid) and after 67 days (dashed). Note that the potential vorticity scale is different from (a).

(ii) The shapes and positions of the induced deep jets (section 6) are insensitive to either parameter. The strength of the positive jet depends on A_H but not on K_H, with the maximum value of $\bar{v}$ increasing from 31 cm s^{-1} to 73 cm s^{-1} as A_H decreases from 400 to 20 m^2 s^{-1}. The negative jet is strengthened by a decrease in either A_H or K_H.

(iii) The energetics as described in section 5 are also qualitatively robust. Decreasing K_H increases the amount of potential energy extracted (by a factor of 2 as K_H decreases from 200 to 20 m^2 s^{-1}), but while a little of this energy goes to increase $\overline{KE}$ (by strengthening the negative jet) most of it is simply dissipated by eddy viscosity. Decreasing A_H not surprisingly decreases the amount of viscous dissipation, but if K_H and A_H are varied together (keeping $A_H = K_H$), the two effects appear to compensate, so that although the other terms in the energy equation change in size, the large scale flow adjusts to dissipate roughly the same amount of kinetic energy. Simmons and Hoskins (1978) obtained a similar result using a biharmonic dissipation term (as opposed to our Laplacian dissipation).

(iv) The final, steady proportion of the total kinetic energy due to the barotropic mode varies between about 0.8 and 0.9. Increasing A_H decreases the proportion, while increasing K_H increases it.

Experiments in which the *vertical* eddy viscosity and diffusivity are varied in the range 10^{-4}–10^{-3} m^2 s^{-1} show that there is very little sensitivity to these parameters.

b. *Experiments in a longer channel*

In all the experiments described so far the channel length M and the wavelength of the initial perturbation have both been chosen to be equal to the wavelength λ_L of the fastest growing linear wave, so that the (periodic) channel has contained only a single wavelength. This precludes nonlinear interactions with longer wavelengths and so leaves open the possibility that the solutions we have described, although mathematically valid, are physically unrealizable because they are unstable to disturbances of longer wavelength.

To examine this possibility we have run an experiment with parameters largely as for experiment SB but with the channel four times as long (i.e., $M = 4\lambda_L$), and with initial state

$$X_0(y) = \overline{X_0} + \epsilon \sin(2\pi y/\lambda_L) + \text{noise}$$

so that the dominant wavelength is still λ_L, but now this fits four times along the channel. The noise field is chosen to give roughly equal kinetic energy in each of wavenumbers 1–3 and 5–8, and so to allow nonlinear interactions between the dominant wavenumber 4 and other wavenumbers.

Figure 15 shows the kinetic energy in wavenumber 4 and in wavenumber 0 (the mean flow) as functions of time. The corresponding energies from the short channel (multiplied by 4) are shown for comparison. We see that the development of the wavelength λ_L (180 km) mode is much the same in the long and the short channels, whereas the development of the mean flow is rather different, with two dips in the long case which were not present in the short runs. Further examination (Wood 1988) shows that the first dip is due to a barotropic instability of the mean flow at wavenumber 3. Baroclinic conversion continues, and this leads to another phase of Reynolds stress convergences feeding energy back into wavenumber 0. The second dip is due to barotropic instability of the new mean flow at wavenumber 2. This cascade of (barotropic) energy to larger scales was also suggested by the results of Orlanski and Cox (1973). It is reminiscent of the quasi-geostrophic turbulence theory of Rhines (1977), but in the present case the cascade is caused specifically by the interaction of successively longer waves with the evolving mean (wavenumber zero) state, rather than by direct interaction between different nonzero wavenumbers. Each successive phase of barotropic instability broadens and

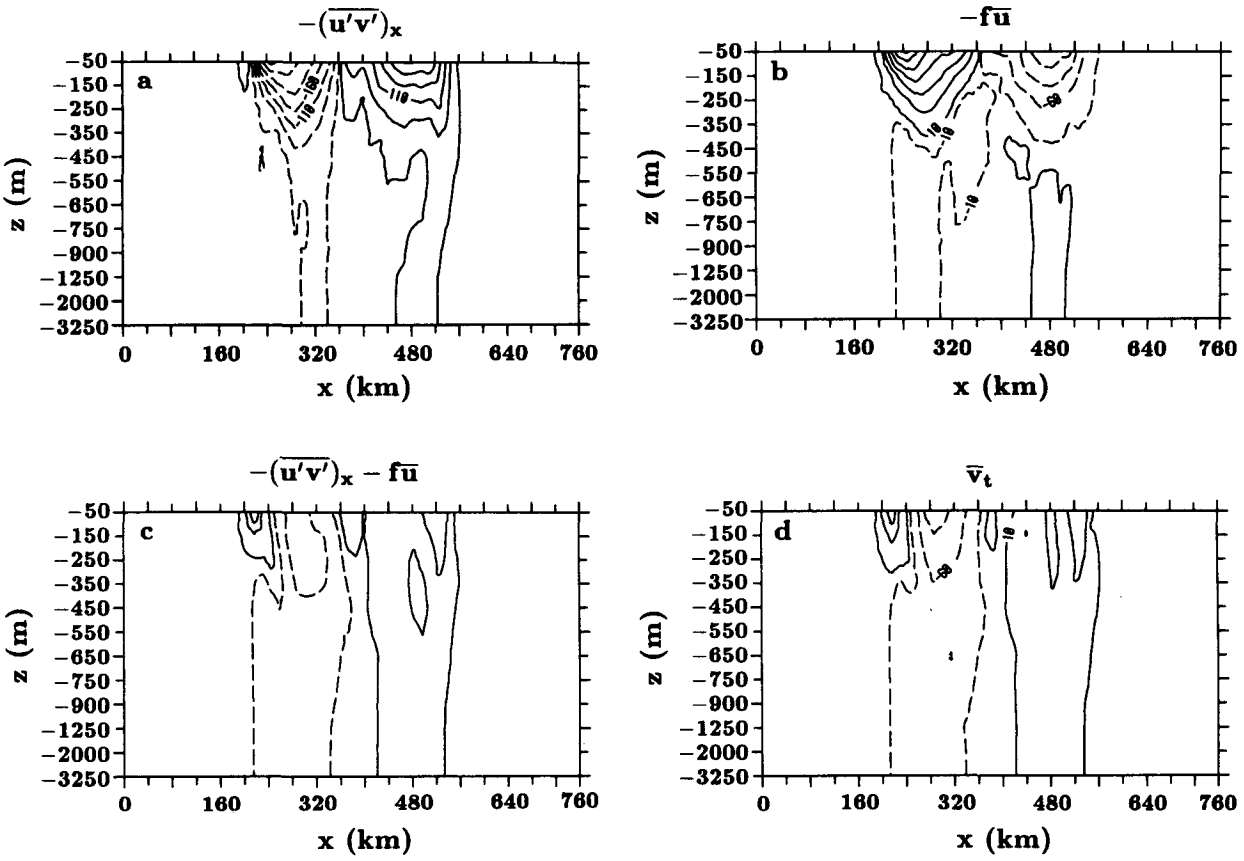

FIG. 14. Terms in the equation of motion (6.1) for the mean velocity $\bar{v}$, for experiment DB after 25 days. Contours at $\pm 1 \times 10^{-7}$ m s^{-2} and then at intervals of 5×10^{-7} m s^{-2}. Contour labels are in units of 10^{-8} m s^{-2}. Dashed contours denote negative values. (a) Reynolds stress divergence $-(u'v')_x$, (b) Coriolis acceleration $-f\bar{u}$, (c) $-(u'v')_x - f\bar{u}$, and (d) $\bar{v}_t$. Note that below 750 m depth the vertical scale has been compressed.

weakens the double jet somewhat, while the Reynolds stress convergence strengthens it. The overall effect of this on the mean flow is shown in Fig. 16.

To summarize, the solutions obtained in the short channel for wavelength λ_L are stable over the first part of the integration, but the (highly barotropized) mean flows which are generated are somewhat barotropically unstable at longer wavelengths, leading to some

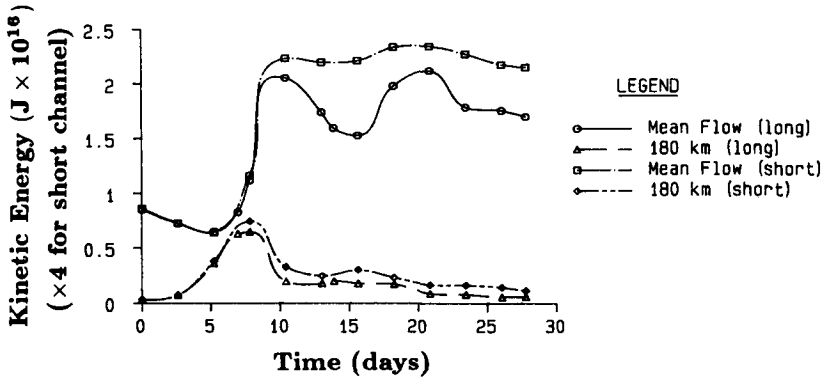

FIG. 15. The kinetic energy in the mean flow (wavenumber 0) and in the linearly fastest-growing mode (180 km wavelength), shown as functions of time for experiment SB (short channel) and for the equivalent experiment in the long channel. The energies for the short channel have been multiplied by 4 to allow direct comparison with the long channel values.

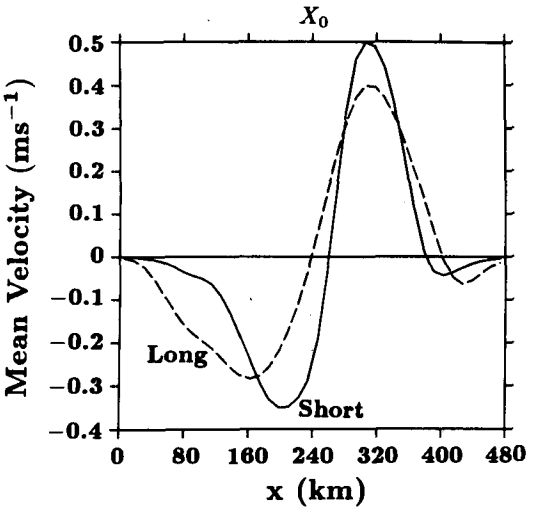

FIG. 16. Mean velocity $\bar{v}$ at 1950 m depth, plotted against the north–south coordinate x after 28 days of integration, for experiment SB (short channel, solid line) and for the equivalent experiment in the long channel (dashed line).

spreading of the double jet structure compared with the short case.

8. Summary and discussion

Our results allow us to identify an energy life cycle for unstable baroclinic waves on an oceanic density front. The first part of the cycle is very robust and consists of a baroclinic growth phase followed by a decay in the potential energy extraction and simultaneously by the generation of mean flows by Reynolds stresses. This agrees well with the results of Simmons and Hoskins (1978) and Ikeda (1981). Subsequent behavior varies somewhat between experiments but we always see a damped oscillatory behavior in the Reynolds stress term ($\overline{KE} \rightarrow KE'$), indicative of vacillation between predominantly barotropic and predominantly baroclinic instability mechanisms. During this stage ($\overline{KE} \rightarrow KE'$) is roughly equal and opposite to ($PE \rightarrow KE'$), so that the potential energy extracted goes largely into the mean flow. The barotropic instability mechanism is enhanced if the system is free to oscillate at wavelengths longer than the wavelength of the initial disturbance.

At small amplitude the waves are well described by the linear theory of Killworth et al. (1984). Finite amplitude effects reduce both the phase speed and the growth rate. The phase speed of the wave crest evolves differently from the phase speed of the trough, with the result that the trough catches up with the crest and the wave adopts a backward breaking shape which is asymmetric about both the north–south and the east–west axes. At large amplitude vortex pairs are formed. These separate from the main front, even when $\beta = 0$, in contrast with Ikeda's (1981) result. This discrepancy is because in Ikeda's quasigeostrophic model β terms dominated the vorticity dynamics, whereas in the present model vortex stretching is much stronger, and is sufficient to induce vortex separation regardless of β. In fact in our model the β-effect tends to trap the cyclonic (but not the anticyclonic) vortex near the front.

The mean flows induced by the disturbance are driven both by horizontal Reynolds stress divergence and by the Coriolis acceleration due to the cross-stream flow. The deep mean flows have a double jet structure, which bears a striking resemblance to Schmitz's (1977) observations under the Gulf Stream. These jets are in fact barotropic and can be seen in the surface flows; one may speculate that large-scale baroclinic forcing mechanisms not present in our model could tend to restore the original frontal jet near the surface while leaving the deep flows unaffected. The jets are somewhat barotropically unstable, particularly at wavelengths longer than the initial wavelength, and this barotropic instability results in a slight spreading of the jets.

The double jet may in fact be an artifact of the periodic boundary condition, in the sense that it results from the self-interaction of the cyclonic vortex. Nonetheless our results remain relevant to the Gulf Stream as quasi-periodic trains of meanders are frequently seen (Hansen 1970). It would be interesting to study the spatial growth of an isolated meander (as in Ikeda and Apel 1981); however this would be both technically difficult (because of the need to develop a suitable open boundary condition at the ends of the channel) and computationally expensive (because of the large domain required).

The β-effect is important in determining the position of the eastward jet to the south of the front; both this and the trapping of the cyclonic eddy can be understood if we think of the cyclonic eddy as acting as a large-scale diffuser of the lower layer potential vorticity (as explained in section 6), but similar arguments do not explain the behavior of the anticyclonic eddy.

As noted by Hogg (1983), the deep velocities in eddy resolving general circulation models (EGCMs) show an eastward mean flow directly below the Gulf Stream axis, with recirculation to the north and south. Ikeda (1981) obtained similar results in his quasi-geostrophic channel model. Our results are, however, closer to what is observed in the ocean, with the eastward flow displaced to the south as observed. The explanation for this discrepancy between the models is not clear. The major differences between our model and Ikeda's are our use of primitive equation rather than quasi-geostrophic dynamics and our asymmetric initial state with a front (as opposed to Ikeda's symmetric jet), so we conclude that the existence of a strong front (which precludes quasi-geostrophic dynamics) can lead to qualitative changes in the induced flow. It would be interesting to know whether asymmetry alone could produce the same change in the quasi-geostrophic

model. It is not straightforward to compare our results with the time-mean flows from EGCMs, in which there is large-scale forcing both by wind stress and by remotely generated wave motions. However it may still be pertinent to point out that EGCM results published to date (e.g., Semtner and Mintz 1977; Holland 1978; Cox 1985) have horizontal grid intervals of order 20–40 km, scarcely sufficient to resolve the Rossby radius a in the vicinity of the Gulf Stream, and that while the dominant length scale of the eddies is rather greater than this, a is still an important scale in the cross-stream direction and eddy dynamics at this scale could influence the mean flow.

Our results show no sign of the deep westward recirculation south of the Gulf Stream observed in the ocean by Schmitz (1977) and in EGCMs, for example, by Semtner and Mintz (1977) and by Holland, Keffer and Rhines (1984). It has recently been proposed (Marshall and Nurser 1986; Greatbatch 1987) that this recirculation may be interpreted as part of a quasi-inertial gyre, closed by inertial boundary currents at the northern, eastern and western boundaries, and restricted, for layers not exposed to wind stress curl forcing, to a region of uniform potential vorticity. Since our model does not have meridional boundaries we would not expect to see such a gyre in our results. The results do however show how, even when the common restriction to quasigeostrophy is relaxed, instabilities of the highly inertial eastward jet tend to homogenize the potential vorticity in the subsurface layers and hence drive the deep flow.

Acknowledgments. I should like to thank Drs. Steve Maskell and Phil Everson for their advice and encouragement during this research, and Professor Robert Haney for his constructive criticism of an earlier version of this paper. Catherine Griffiths and two anonymous reviewers also made several helpful suggestions. The financial support of the Science and Engineering Research Council is also gratefully acknowledged.

REFERENCES

Apel, J. R., 1980: Satellite sensing of ocean surface dynamics. *Ann. Rev. Earth Planet. Sci.*, **8**, 304–342.

Bryan, K., 1969: A numerical method for the study of the circulation of the world ocean. *J. Comput. Phys.*, **4**, 347–376.

Cooper, N. S., 1986: A comparison between a layer model and a global circulation model: Thermocline depth and Kelvin wave speed. Dept. of Atmospheric Physics, Clarendon Laboratory, Oxford, U.K., (unpublished manuscript).

Cox, M. D., 1985: An eddy resolving numerical model of the ventilated thermocline. *J. Phys. Oceanogr.*, **15**, 1312–1324.

Fuglister, F. C., and L. V. Worthington, 1951: Some results of a multiple ship survey of the Gulf Stream. *Tellus*, **3**, 1–14.

Garvine, R. W., 1984: Propagating long waves on oceanic density fronts: An analytic model. *J. Phys. Oceanogr.*, **14**, 1590–1599.

Greatbatch, R. J., 1987: A model for the inertial recirculation of a gyre. *J. Mar. Res.*, **45**, 601–634.

Griffiths, R. W., and P. F. Linden, 1981: The stability of vortices in a rotating, stratified fluid. *J. Fluid Mech.*, **105**, 283–316.

——, and ——, 1982: Laboratory experiments on fronts. Part 1: Density-driven boundary currents. *Geophys. Astrophys. Fluid Dyn.*, **19**, 159–187.

Halliwell, G. R., and C. N. K. Mooers, 1983: Meanders of the Gulf Stream downstream of Cape Hatteras. *J. Phys. Oceanogr.*, **13**, 1275–1292.

Hansen, D. V., 1970: Gulf Stream meanders between Cape Hatteras and the Grand Banks. *Deep-Sea Res.*, **17**, 495–511.

Hogg, N. G., 1981: Topographic waves along 70°W on the continental rise. *J. Mar. Res.*, **39**, 627–649.

——, 1983: A note on the deep circulation of the western north Atlantic. *Deep-Sea Res.*, **30**, 945–961.

Holland, W. R., 1978: The role of mesoscale eddies in the general circulation of the ocean—numerical experiments using a wind-driven quasi-geostrophic model. *J. Phys. Oceanogr.*, **8**, 363–392.

——, and P. B. Rhines, 1980: An example of eddy-induced ocean circulation. *J. Phys. Oceanogr.*, **10**, 1010–1031.

——, and M. L. Batteen, 1986: The parameterisation of subgrid-scale heat diffusion in eddy-resolved ocean circulation models. *J. Phys. Oceanogr.*, **16**, 200–206.

——, T. Keffer and P. B. Rhines, 1984: Dynamics of the ocean general circulation: the potential vorticity field. *Nature*, **308**, 698–705.

Ikeda, M., 1981: Meanders and detached eddies of a strong eastward flowing jet using a two layer quasi-geostrophic model. *J. Phys. Oceanogr.*, **11**, 526–540.

——, and J. R. Apel, 1981: Mesoscale eddies detached from spatially growing meanders in an eastward flowing oceanic jet using a two layer quasi-geostrophic model. *J. Phys. Oceanogr.*, **11**, 1638–1661.

James, I. D., 1984: A three-dimensional numerical shelf-sea front model with variable eddy viscosity and diffusivity. *Contin. Shelf Res.*, **3**, 69–98.

Killworth, P. D., 1983: Long-wave instability of an isolated front. *Geophys. Astrophys. Fluid Dyn.*, **25**, 235–258.

——, N. Paldor and M. E. Stern, 1984: Wave propagation and growth on a surface front in a two-layer geostrophic current. *J. Mar. Res.*, **42**, 761–785.

Levine, E. R., D. N. Connors, P. C. Cornillon and H. T. Rossby, 1986: Gulf Stream kinematics along an isopycnal float trajectory. *J. Phys. Oceanogr.*, **16**, 1317–1328.

Luyten, J. R., 1977: Scales of motion in the deep Gulf Stream and across the continental rise. *J. Mar. Res.*, **35**, 49–74.

Marshall, J., and G. Nurser, 1986: Steady, free circulation in a stratified quasi-geostrophic ocean. *J. Phys. Oceanogr.*, **16**, 1799–1813.

Orlanski, I., and M. D. Cox, 1973: Baroclinic instability in ocean currents. *Geophys. Fluid Dyn.*, **4**, 297–332.

Paldor, N., 1983: Linear stability and stable modes of geostrophic fronts. *Geophys. Astrophys. Fluid Dyn.*, **24**, 299–326.

Phillips, N. A., 1956: The general circulation of the atmosphere: a numerical experiment. *Quart. J. Roy. Meteor. Soc.*, **82**, 123–164.

Pratt, L. J., and M. E. Stern, 1986: Dynamics of potential vorticity fronts and eddy detachment. *J. Phys. Oceanogr.*, **16**, 1101–1120.

Rhines, P. B., 1977: The dynamics of unsteady currents. *The Sea*, Ed. E. D. Goldberg and co-editors, Vol. 6, Academic Press, 603 pp.

Schmitz, W. J., 1977: On the deep general circulation in the western north Atlantic. *J. Mar. Res.*, **35**, 21–28.

Semtner, A. J., and Y. Mintz, 1977: Numerical Simulation of the Gulf Stream and mid-ocean eddies. *J. Phys. Oceanogr.*, **7**, 208–230.

Simmons, A. J., and B. J. Hoskins, 1978: The life cycles of some nonlinear baroclinic waves. *J. Atmos. Sci.*, **35**, 414–432.

Simpson, J. H., 1981: The shelf-sea fronts—implications of their existence and behaviour. *Phil. Trans. Roy. Soc. London*, **A302**, 531–543.

Stommel, H., 1966: *The Gulf Stream*. University of California Press, 248 pp.

Wood, R. A., 1988: Instability of Oceanic Fronts. Ph.D. thesis, University of Exeter, 219 pp.